Original Article	*Curr. Appl. Sci.*, **2022**, *2*(1):31-48 DOI:10.22034/cas.2022.346726.1024	Current Applied Sciences

Preparation of pH-Responsive Vesicular Doxorubicin: Evidence from In-Vitro and In-Silico Evaluations

Saman Sargazi[1], Mahmood Barani[2]*, Farshid Zargari[3], Rabia Arshad[4], Rakesh K. Sharma[5]

[1] *Cellular and Molecular Research Center, Research Institute of Cellular and Molecular Sciences in Infectious Diseases, Zahedan University of Medical Sciences, Zahedan 9816743463, Iran*
[2] *Medical Mycology and Bacteriology Research Center, Kerman University of Medical Sciences 76169-13555, Kerman, Iran*
[3] *Department of Chemistry, Faculty of Science, University of Sistan and Balouchestan, Zahedan, Iran*
[4] *Department of Pharmacy, Quaid-i-Azam University, Islamabad 45320, Pakistan*
[5] *Applied Chemistry Department, Faculty of Technology and Engineering, The M. S. University of Baroda, Vadodara, Gujarat, India*
Corresponding author's e-mail: *mahmoodbarani7@gmail.com*

Article Information

Received: 11 June 2022
Revised: 27 June 2022
Accepted: 28 June 2022
Published online: 17 July 2022

Keywords

Doxorubicin
Niosomes
In-silico analysis
Nanocarrier
pH-Responsiveness
Vesicle

Abstract

Colloidal nanocarriers have provided great opportunities in the field of drug delivery. In this study, to achieve the efficient delivery of anti-cancer agents at the site of action, doxorubicin (DOX) was encapsulated within pH-responsive ergosterol-modified niosomes. The niosome-based formulation displayed size of 125 nm, a surface charge of -22.7 mV, a DOX encapsulation efficiency (EE) of 70.8%, and pH-responsive release behavior. An *in-silico* approach was conducted to analyze the interactions of the loaded drug with the niosome bilayer and to evaluate the structural and dynamical properties of the loaded nanovehicle by constructing a niosome bilayer model containing Tween 60, Span 60, and ergosterol molecules. Computational analyses revealed that the α-hydroxy ketone and daunosamine moieties of DOX are responsible for its arrangement towards the niosome bilayer. On the other hand, the cytotoxic activity of encapsulated DOX compared with its free form in an MCF7 breast cancer cell line was evaluated. Compared with free administered DOX, we found lower IC50 values for the MCF7 cells exposed to niosomal DOX (1.153 vs. 0.229 after 24 h, 0.796 vs. 0.148 µg/mL after 48 h, and 0.461 vs. 0.081 µg/mL after 72 h of incubation, respectively). Additionally, niosomal DOX-induced apparent morphological alterations in MCF7 cells. Hence, we showed that niosomes are promising nanocarriers that can be used to encapsulate and release well-established anti-cancer drugs in order to improve their release and, thus biological activity and therapeutic efficacy.

1. Introduction

Among all therapeutic strategies, anti-estrogen therapy can be considered one of the most optimal for treating hormone-receptor-positive cancers [1]. Doxorubicin (DOX) is able to counteract the effects of estrogen via increasing the levels of specific growth factors signaling molecules [2, 3]. However, the marketed oral formulations of DOX suffer from gastric instability as well as extensive first-pass effect, requiring large administered dose concentrations, which result in dose-dependent side effects and significant inter-individual variations [4]. Moreover, the physical barrier to drug diffusion and insufficient drug concentration delivery within the tumor area is also very challenging. In addition, the heterogeneity of tumors also reduces the therapeutic efficacy of the administered drug, making it necessary to envisage ways to target tumors more selectively [5].

The advent of nanotechnology helped in designing novel nanocarriers for targeted drug delivery, imaging, and theranostic applications [6-8]. The most common methodology of targeted therapy to the tumor area for the selective release of an encapsulated hydrophobic drug within a nanocarrier of suitable size is passive targeting by means of the enhanced permeation and retention effect (EPR). Many nanocarriers, such as liposome, microemulsions, missiles, inorganic nanomaterials, etc., were developed for anti-cancer therapy [9]. Lipid-based nanocarriers are useful vehicles for entrapping hydrophobic drugs and being concentrated in the tumor area thanks to their nanometer size and composition mimicking that of cell membranes [10, 11]. They have been previously used to efficiently load anti-cancer agents, particularly DOX [12-15]. However, the high cost of preparation, multiple synthetic steps, inadequate drug loading, and release profiles, difficulties for large-scale production, early clearance from the body, etc. challenges, still have to be solved [16]. Recently, niosomes have drawn great attention to pharmaceutical technology and anti-cancer drug delivery because of their thermodynamic and kinetic stability, biodegradability, biocompatibility, non-immunogenicity, and ease of preparation, as well as the distinctive quality for solubilizing hydrophobic agents. In this connection, several studies have been conducted to efficiently deliver DOX, as an anthracycline agent, to cancer cells. It has been previously reported that modification of gold nanoparticles through covalent conjugation with polyethylene glycol (PEG) enhanced the bioavailability of DOX for the treatment of osteosarcoma. Moreover, we have previously shown that entrapment of DOX within lignin-based DOX-loaded oil-in-water nanomicelles enhanced its anti-cancer effects against tumor cells without noticeable effects on non-cancerous human cells [17]. Similarly, we observed that Pluronic F127/Doxorubicin microemulsions induced marked morphological changes and cell-killing effects in MCF-7 and C152 oral carcinoma cells. *In-vivo* examinations showed that this nanodrug induced fatty changes and increased serum liver enzymes in rats [18]. These reports provided the rationale for DOX-loaded colloidal nanoassemblies' safety profile and their application in cancer therapy. More studies should be performed to determine the *in-vivo* efficacy of lipid-based nanoformulations and overcome the pharmacokinetic limitations of standard DOX before clinical use.

To even enhance physiological stability, some additives can be incorporated into the niosome structures, such as ergosterol [19]. On the other hand, a targeting strategy can be complemented with additional strategies, for example, to control the release of the antineoplastic drug from the nanovehicle. To this end, a pH-responsive triggering mechanism has been widely appealing to achieve a localized drug release within the tumor environment, provided that the differences in pH between healthy and tumoral environments [20].

Taking all together, we here developed highly specific DOX-encapsulated, ergosterol-modified pH-responsive niosomes to trigger DOX drug release [21, 22] in order to achieve optimal therapeutic concentrations at the targeted site. Thus, preventing cancer progression at lower administered dose concentrations [23]. Furthermore, ergosterol

was employed instead of cholesterol in the niosome structure. We determined the *in vitro* efficacy of niosomal-encapsulated DOX compared to the free administered drug in a MCF7 breast cancer cell line, being observed with lower IC50 values in the former case than in the latter. Moreover, synthesized DOX-loaded niosomes exhibited favorable cytotoxic effects against breast cancer cells. To the best of our knowledge, the current study is the first one to report the preparation of specified DOX-encapsulated pH-responsive niosomes modified with ergosterol to induce cytotoxic effects against cancerous cells.

2. Materials and Methods

2.1 *Chemicals and reagents*

Doxorubicin hydrochloride injectable solution (2.5 mg/mL) was provided by EBEWE Pharma (Unterach am Attersee, Austria). Cholesteryl hemisuccinate (CHEMS) was obtained from Avanti Polar Lipids, Inc (Ala-baster, Alabama, USA). RPMI1640, fetal bovine serum (FBS), and 0.25% trypsin-EDTA solution were obtained from Gibco (Grand Island, NY, USA). Penicillin, streptomycin, MTT dye, phosphate-buffered saline (PBS), dimethyl sulfoxide (DMSO), ergosterol, Span 60, Tween 60, and trypan blue were from Sigma-Aldrich (Steinheim am Albuch, Germany and St Louis, MO, USA). The MCF7 cells were purchased from the cell bank of Pasteur Institute of Iran (Tehran, Iran), cultivated in RPMI1640 medium supplemented with 10% FBS, 1% penicillin/streptomycin solution, and kept under standard conditions (5% CO_2, 95% air, 37°C). Phosphate buffer solutions of pH 7.4 and 5.4 were prepared according to Eur. Pharm. 6th Ed. Ultrapure water was used throughout the study.

2.2 *Synthesis of pH-responsive DOX-Niosomes*

The thin-film hydration or TFH approach was used to make the niosomes. In a round-bottom flask with a total concentration of 300 μM, lipid composition was dissolved in chloroform that included accurately weighed volumes of Tween 60, ergosterol, Span 60, and CHEMS with a molar ratio of 0.35:0.30:0.35: 0.1. A rotating evaporator was used to evaporate the chloroform used as solvent under a vacuum at 60 ºC (Laboroa 4003, Heidolph, Germany). The thin film was then hydrated in the rotary evaporator at the same temperature, with 5 mL of DOX aqueous solution (83 ppm) once completely free of the organic solvent. The obtained suspension appears to be a low viscosity milky-reddish fluid.

2.3 *Reduction of niosomes size*

Niosomal suspensions (obtained according to the above-described methods) were centrifuged for 20 min at 15000 rpm (5415D centrifuge, Eppendorf, Germany) to separate unencapsulated drugs. Then precipitations were dispersed in water and sonicated (Fisherbrand™ Model 50 Sonic Dismembrator, USA) for 5 min, with the instrument set at 60% of its maximum power. Afterward, the suspension was filtered five times with filters of 0.45 and 0.22 um (Sartorius AG, Göttingen, Germany). All the samples were stored at 4°C and protected from the light.

2.4 *System setup and simulation details*

The structure of the bilayer niosome components, such as Span 60, Tween 60, ergosterol, and DOX, were obtained from the PUBCHEM website. The structure was optimized first at the B3LYP/6-3G(d,p) level of theory. Using the CELL microcosmos 2.2 software, each optimized structure (shown in Figure 1) was used to create a niosome bilayer at a 35:35:30 molar ratio of Span 60:Tween 60:ergosterol. This bilayer model included up to ca.

80 Tween 60, 82 Span 60, and 70 ergosterol molecules, which were arbitrarily arranged in a box diameter of 4.50 nm and with hydrophilic heads towards one another inside the box.

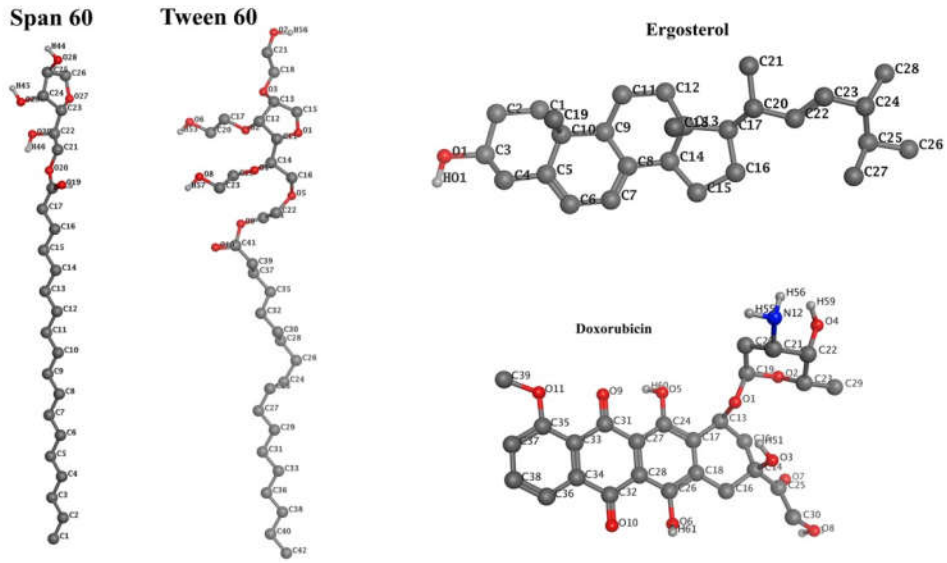

Figure 1. Molecular structures of DOX, Span 60, Tween 60, and ergosterol with the numbering of atoms following the amber nomenclature

To distinguish it from its last configuration, as seen in Figure 2a, the DOX molecule's initial configuration was considered as composed of five molecules placed on the top of the bilayer. We used the SPC/E model of water since it is thought that it can provide water surface tension more accurately [24]. Using both Gromos87 [25] and Gromos96 54a7 force field [26], the bounded and non-bounded parameters for all components of the niosome were obtained using the ATB server [27]. To avoid unforeseen collisions and overlaps in the model, the steepest descent algorithm was utilized. To remove any remaining overlaps between atoms, an ordered cooling, and heating operation in the region of 298 to 500 K was used. In addition, to reach equilibrium conditions set up at 298 K and 1 bar, a 500 ps in a constant number of particles (N), volume (V), and temperature (NVT) ensemble followed by a 10 ns simulation in a constant number of particles (N), pressure (P), and temperature (NPT) was performed. The temperature was chosen to meet the parameters for optimal niosome generation and stabilization [28]. The Span 60, Tween 60, and ergosterol coupling groups were supplied to the v-rescale thermostat and all coupled together with a coupling constant of 0.1 ps. In contrast, water and DOX molecules were associated independently. The Berendsen barostat with semi-isotropic coupling was used to maintain the system's temperature and pressure at 298 K and 1 bar, respectively. In all three space directions, periodic boundary conditions were applied. During MD simulation [29], the LINCS algorithm was also used to limit the bonds and the Fast Particle Mesh Ewald method (PME) to control the electrostatic interactions [30]. Coulomb and van der Waal interactions taking place at distances longer than 1.5nm were not taken into account. Gromacs 2020.1 was also used to simulate the system for 40 ns. Figure 2b represents the final structure of the bilayer following this 40-ns MD simulation with the antineoplastic drug.

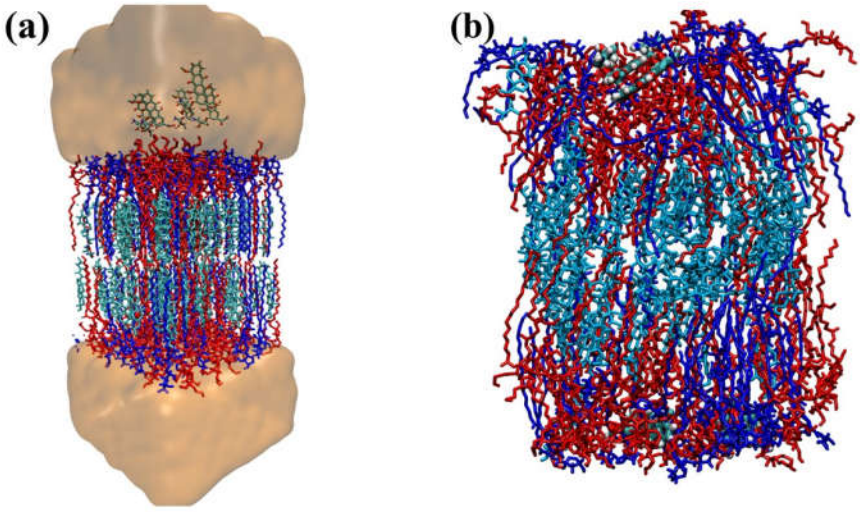

Figure 2. (a) Starting configuration of MD simulation with DOX drug molecules at the upper leaflet. The color map for bilayer components is green, purple, and orange for Span 60, Tween 60, and ergosterol, respectively. (b) Niosome configuration after 40 ns of MD simulation

2.5 ***Characterization of DOX-encapsulated niosomal formulations***

2.5.1 *Morphology*

Both optical microscopy (before size reduction) and TEM (after size reduction) imaging were done to analyze the architecture of hydrated niosomal dispersions. For TEM, a drop of the dispersion was layered onto a carbon-coated copper grid and allowed to adhere for roughly 1 min. The filter paper was used to eliminate the remaining traces of liquid dispersion. A drop of 2% (v/v) phosphotungstic acid solution was added, and the excess solution was discarded with filter paper once again. The sample was air-dried before being examined using a TEM microscope (LEO912-AB, Zeiss, Germany). Also, a drop of the formulation was mounted on a coverslip and observed using an optical microscope (Leica, ICC50 W, Germany) to visualize the appearance of vesicles before filtration.

2.5.2 *Size and Zeta potential*

A Zetasizer Nano instrument (Malvern, ZEN3600, UK) was used to assess the niosome zeta potential, polydispersity index, and sizes at 25 °C by monitoring the autocorrelation function at 90°. A solid-state 35 mW laser operating at 658 nm was used as the light source. The polydispersity index reveals the dispersion size quality, with values less than 0.3 indicating good monodispersity of the formulations. Each experiment was repeated at least three times.

2.5.3 *Entrapment efficiency of DOX-loaded niosomes*

The percentage of DOX entrapped inside the niosomes compared to the total amount of drug was used to calculate the DOX encapsulation efficiency. Firstly, non-encapsulated Dox was separated from encapsulated ones with a centrifuge at 15000 rpm for 30 minutes (5415D, Eppendorf, Germany). Following the separation technique, the proportion of DOX enclosed was estimated for this purpose. DOX content in the supernatant was evaluated in triplicate at 480 nm using a UV-visible Spectro-photometer (Cary 50, Agilent Technologies, USA).

2.6 *Release profiles*

A dialysis tube was filled with DOX-loaded pH-responsive niosomes (12 kDa membrane cutoff; Sigma-Aldrich, USA). Niosomal formulations were mixed at 37 °C in a beaker containing 100 mL of PBS (pH 7.4 or 5.4). Samples were taken at predetermined intervals and examined using a UV–vis spectrometer set to 480 nm. Fresh equal volumes of buffer were added after the removal of the suspension aliquots taken out for analysis in order to maintain sink conditions. Release data were calculated as the average of three different runs. The *in-vitro* release of free DOX was used as a control.

2.7 *Cell culture conditions and viability assay*

Cells (5000 cells/well) were seeded in a 96-well microplate and, following an overnight incubation, treated with increasing concentrations of free and DOX-encapsulated niosomes (0, 0.075, 0.15, 0.3, 0.6, and 1.2 µg/mL DOX) for 24, 48, and 72 h. Then, cells were washed with PBS, and 200 µL of MTT reagent (0.5 mg/mL) were placed into each well and kept in an incubator for another 4 h. Next, the supernatant was replaced with 200 µL of DMSO in order to dissolve the formazan crystals. The reduced MTT was assayed at 570 nm using a plate reader. Wells with untreated cells were considered as controls, and the experiment was performed in triplicate. Cell viability was calculated as (OD_{570} of treated cells/OD_{570} of control cells) × 100. Using an inverted microscope, we also observed the morphological changes in MCF7 cells treated with given concentrations of free and DOX-loaded niosomes after 48 h of incubation.

3. Results and Discussion

3.1 *Physicochemical characterization of niosomal DOX*

The use of traditional chemotherapeutics has several limitations, including lengthy treatment periods, severe side effects, and the potential appearance of drug resistance. Drug delivery nanosystems have been designed to allow the administration of lower total doses supplied to patients by increasing the drug/carrier circulation time, enhancing drug stability, and reaching a targeted preferential distribution of the therapeutic cargo in the site of action. In this regard, to integrate the benefits of reduced uptake by the mononuclear phagocyte system and subsequently achieve longer circulation times, we here developed pH-responsive niosomal-based drug delivery vehicles. Furthermore, ergosterol was employed instead of cholesterol in the niosome structure. Based on our previous studies, the use of ergosterol instead of cholesterol can enhance the properties of developed niosomes [31]. Tween 60, ergosterol, and Span 60 were used to make these new pH-responsive niosome formulations, which are suited for targeted application due to pH-dependent release. Tween 60 and Span 60 are nonionic surfactants made up mostly of fatty acid esters of sorbitol-derived cyclic ethers (sorbitans and sorbides). They have been utilized to give flavor to various foods, cosmetics, and pharmaceuticals. On the other hand, ergosterol (ergosta-5,7, 22-trien-3-ol) is a sterol present in protozoa and fungi cell membranes that behave similarly to cholesterol in mammalian cells. The shape and length of cholesterol and ergosterol are somehow similar. A planar cyclopentane-phenanthrene ring, a 3-OH group, and a hydrophobic side-chain connected to C17 are all common characteristics. Thus, adding ergosterol to a carrier may enhance its pharmacokinetic and physicochemical characteristics.

In order to establish a new carrier nanosystem for cancer therapy, pH-responsive DOX-niosomal vesicles were produced and characterized in this study (Figure 3a). Before size reduction, niosomes were examined in an optical

microscope with a 100X objective. Optical images showed the formation of niosomes with micrometer dimensions and a multilamellar structure (Figure 3b). As observed in Figure 3c, TEM images also reveal the well-defined spherical geometry of the obtained niosomes after size reduction, with a diameter of ca. 120 nm and with a smooth surface.

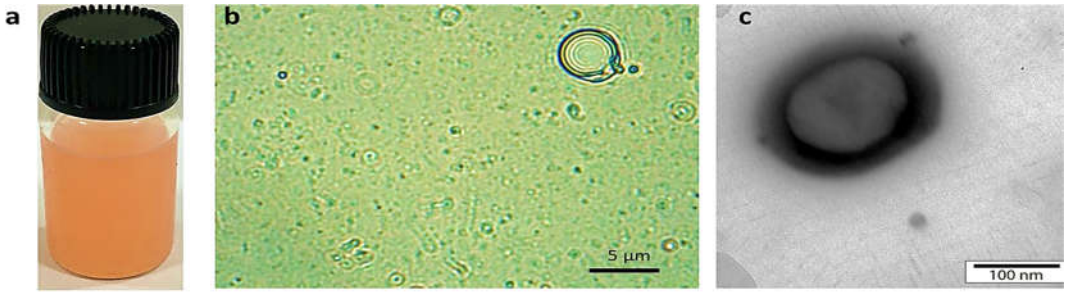

Figure 3. Sample appearance (a), optical microscopy (b), and TEM image (c) of pH-responsive niosomal DOX

Dynamic light scattering was used to determine the zeta potential, size, and population size distribution of niosome formulations. The resulting hydrodynamic diameters and polydispersity indices are given in Figure 4. The mean hydrodynamic diameter of drug-loaded niosome vesicles after size reduction was 125 nm with a 0.21, rather similar that obtained by TEM imaging. A PDI <0.3 indicated that the obtained DOX-loaded niosomes are relatively monodisperse and without signs of aggregation, then leading to a stable formulation [32-34]. The boundary between potential aggregation and a stable suspension results from a balance between short-range effective, attractive interactions and electrostatic repulsion due to the non-uniform charge distribution at the particle surfaces [35, 36]. In this regard, the obtained pH-responsive DOX-loaded niosomes possess a zeta potential of -22.7 mV, sufficient to provide electrostatic-based stability to the formulation.

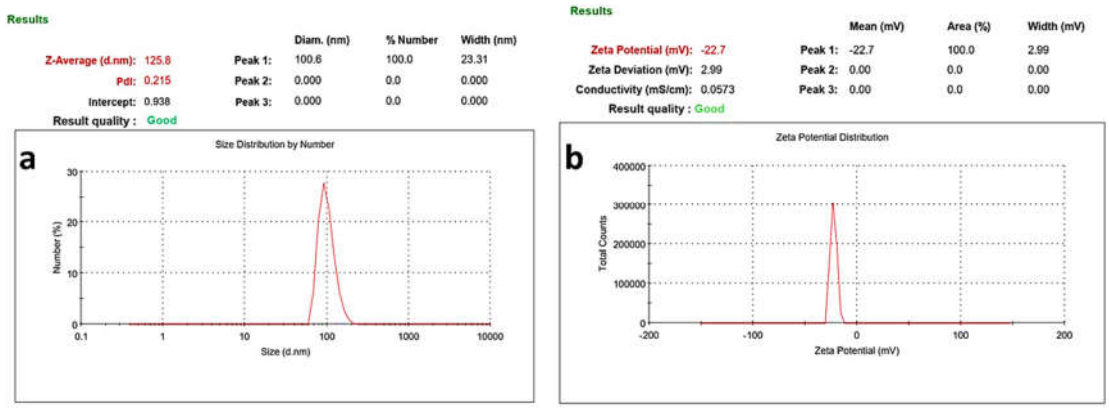

Figure 4. Size (a) and zeta potential (b) distributions of pH-responsive DOX-loaded niosomes measured by DLS and Doppler anemometry

3.2 *Niosome bilayer structure*

The structural and dynamical properties of the niosome bilayer were evaluated using an atomic bilayer model made up of Tween 60, Span 60, and ergosterol. MD simulations were also used to investigate the APL and thickness of the derived niosome bilayer. Using APL as a dynamical characteristic of the bilayer, we observed that Span 60 is essential for maintaining the APL value constant, whereas both Tween 60 and ergosterol had no effects.

We additionally identified that DOX molecules are prone to dimerization at the bilayer-solvent interface. This is because their naphthacene moieties adopt a unique conformation in which the aromatic rings form strong π- π or π-alkyl contacts with them together. According to the data, DOX molecules interact with the lipid bilayer primarily by forming strong hydrogen bonds with Span 60 and Tween 60 headgroups mainly involving the primary and tertiary alpha-hydroxy ketone (O7 and O8 atoms) and daunosamine (O4 atom) moieties of DOX. An RDF analysis was additionally performed to provide a significant structural understanding of the interactions during Dox-loaded niosomes production. The RDF plots obtained were consistent with strong hydrogen bonding and indicated that DOX is arranged in the bilayer boundaries by its alpha-hydroxy ketone and daunosamine moieties.

In previous works, we used the GridMAT-MD script [37] to evaluate the area per lipid (APL) and bilayer thickness of the Span60:Tween60:ergosterol system in a 35:35:30 molar ratio. Thus, we constructed/simulated the niosome bilayer structure following a similar procedure. By using the same compositions and the same forcefield parameters, it is more likely to get the same results for APL and bilayer thickness in contact with DOX in the present work. The average value of APL for Span 60 was 24.7 ± 0.1 $Å^2$ at the beginning of the MD simulation, while this value diminished to 22.3 ± 0.1 $Å^2$ at the end, in line with the experimental value (22 $Å^2$) [38]. We showed that the APL did not expand drastically by introducing Tween60 and ergosterol to the closely packed system with a high order orientation of Span 60 molecules. In addition, Tween 60 and ergosterol possessed an average APL of 22.8± 0.1 and 26.1 ± 0.1 $Å^2$ after 40 ns MD simulation. Moreover, in the case of the bilayer thicknesses, the calculated ones for Span 60, Tween 60, and ergosterol were 5.920 ± 0.001, 6.950 ± 0.001, and 2.850 ± 0.001, respectively.

3.3 *Aggregation of DOX at the bilayer-solvent niosome interface*

It has been reported that DOX can form dimers and higher-order oligomers, which are believed to be highly sensitive to the medium pH [39-41]. Previous reports suggested that dimerization dominates at low DOX concentrations, especially at pH values where the uncharged form of the drug is prevailing. Figure 5a illustrates the formation of DOX dimerization at the surface of our niosome bilayer model. It is not surprising to observe this phenomenon due to the planar aromatic chromophore section of the molecule. It can be seen from Figure 5b that the aromatic rings in the naphthacene moieties of the two DOX molecules are rearranged so that their planar parts make strong π- π or π-alkyl interactions with each other, leading to their dimerization at the surface of the bilayer.

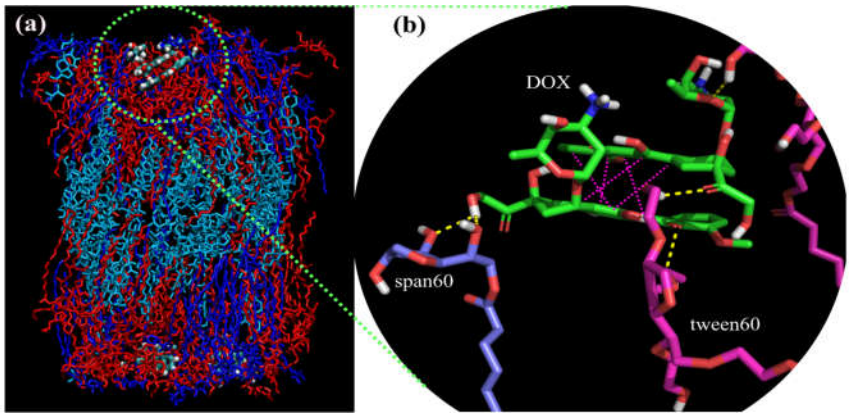

Figure 5. (a) Structure of DOX at the edge of the lipid bilayer as a facial illustration, and (b) close-up illustration of DOX dimerization at the bilayer surface and the most probable hydrogen bonding between DOX and bilayer constituents. Span 60, Tween 60, and DOX are colored blue, purple, and green, respectively

3.4 *Radial distribution function analysis*

The configurations of the DOX molecule in bulk and at the bilayer surface are governed by a few forces. Average radial distribution functions (RDF) plots of DOX, Span 60, Tween 60, and ergosterol were used to examine such types of interactions, which may help in providing additional structural insights. RDF plots are shown in Figure 6. Using MD simulation, the binding mode of DOX molecules towards the bilayer can indeed be determined by comparing critical atoms of DOX with those belonging to the headgroups of bilayer subunits.

DOX consists of a daunosamine group joining naphthacene rings by a primary and tertiary alpha-hydroxy ketone. We performed RDF calculations for O4 in daunosamine, O7 in alpha-hydroxy ketone, and O10 and O11 in naphthacene towards headgroups atoms of Span 60 to evaluate the arrangement of every portion (O19, O28, and O29). The O4 atom in the daunosamine moiety of DOX was fully considered in the RDF calculation based on the hydrogen bonding criterion for Tween 60. As shown in Figures 6a and 6b, the most intense RDF peaks are those corresponding to O4 interactions in the daunosamine moiety of DOX with O29 and O7 atoms of Span 60 and Tween 60, respectively. The remaining critical interactions, being of lower strength, occur here between O28 and O29 atoms of the Span 60 headgroup and the O7 atom of the alpha-hydroxy ketone in DOX, as shown in Figure 6a. Atom O7 is the second one most interacting in Tween 60, just after the O7 atom of the alpha-hydroxy ketone in DOX. The atomic RDF of ergosterol with DOX is shown in Figure 6c. The unique possible but least accurate interaction of the two species in the box involves O1 atom in ergosterol and O10 one in DOX, shown in Figure 6c. DOX and bilayer components (Span 60 and Tween 60 headgroups) interact mainly with each other through the daunosamine and alpha-hydroxy ketone moieties in DOX. Because these interactions are within the spectrum of hydrogen bond formation, it is not surprising to observe them in Table 1, and also in Figure 5b.

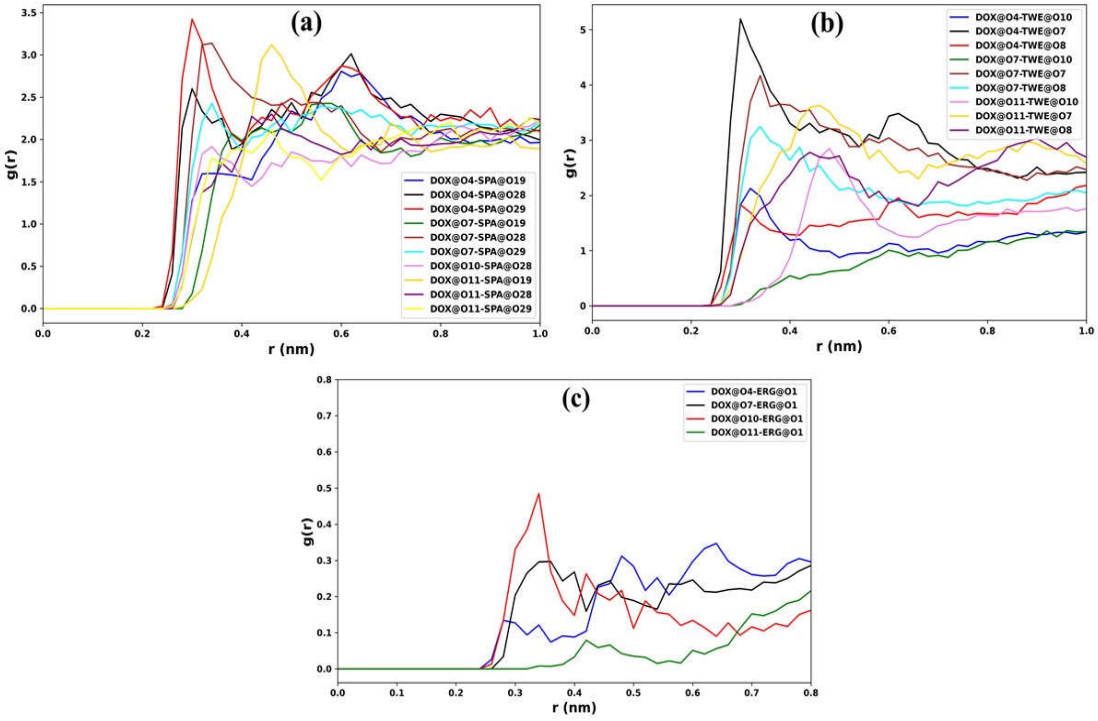

Figure 6. Atom-atom RDFs of (a) Span 60 and (b) Tween 60 headgroup atoms with those of DOX molecules (Atom numbering corresponds to Figure 1)

3.5 *Hydrogen bonding between lipidic membrane and DOX*

We performed hydrogen bonding analysis for 40 ns of trajectory to determine the amount and/or duration of hydrogen bonds generated between the three components of the niosome bilayer, -Span 60, Tween 60, and ergosterol with DOX. The G bond function in Gromacs 2020.1 was used to compute the H-bond profile among DOX and the surfactants and lipids. The H-bond formation cutoff was 3.5 at 30°.

By monitoring hydrogen bond-formation throughout MD simulation, DOX molecules were observed to be located near the bilayer boundary, as seen in Figure 3a. The DOX molecules are connected to Span 60, Tween 60, and ergosterol as observed in Figure 3b. Table 1 shows that DOX has a substantially weaker interaction with ergosterol (average hydrogen bond of 0.03) than the other bilayer components. The longer distance between these two molecules indicates the preference of ergosterol to interact by hydrogen bonding with Span 60 and Tween 60 through its headgroup [42]. The most energetic hydrogen bonding is irresponsible for most DOX-bilayer interactions via Tween 60 and Span 60 headgroups. The occupancy values for the lifespan of the hydrogen bonding between O19 and O28 atoms of Span 60 and O7 and O8 atoms of the main and tertiary alpha-hydroxy ketone in DOX constitute proof for such a statement (Figure 1a). Hydrogen bonds between DOX and the Tween 60 headgroup were also noteworthy. The most important atoms of Tween 60 are O6, O7, and O8, which establish H-bond interactions with O4 and O7 atoms of DOX (Figure 1a). Finally, DOX generates the strongest hydrogen bonds with Span 60 and Tween 60 by means of its O8 and O4 atoms in the tertiary alpha-hydroxy ketone and daunosamine moieties, respectively, as shown in Table 1.

Table 1. Average and detailed hydrogen bond analysis of DOX with Span 60, Tween 60, and ergosterol

	Hydrogen Bonds					
	DOX-Span 60		**DOX-Tween 60**		**DOX- ergosterol**	
Average hydrogen number	1.28		1.38		0.03	
Detailed hydrogen bonds	Donor-Acceptor	Occupancy	Donor-Acceptor	Occupancy	Donor- Acceptor	Occupancy
	DOX@O8-SPA@O19	7.42	TWE@O7-DOX@O4	6.37	ERG@O1-DOX@O10	0.65
	SPA@O28-DOX@O7	5.42	TWE@O8-DOX@O7	5.20	ERG@O1-DOX@O3	0.62
	SPA@O28-DOX@O2	5.22	TWE@O6-DOX@O7	5.17	ERG@O1-DOX@O7	0.52
	DOX@O8-SPA@O28	4.70	TWE@O7-DOX@O7	5.17		

SPA: Span 60; TWE: Tween 60; ERG: ergosterol; DOX: Doxorubicin

3.6 *Entrapment efficiency*

Encapsulation efficiency and drug loading are critical properties for drug delivery systems, especially for expensive, toxic and hydrophobic drugs like DOX, in order to achieve optimal localized therapeutic concentrations at much lower total administered doses while avoiding adverse side effects. It is worth noting that the concentration of entrapped DOX may be determined by its affinity for surfactants, i.e., the encapsulation of water-soluble compounds may be influenced by the bilayer composition. The encapsulation efficiency of DOX was approximately 70.8%. With such a high EE%, Span 60 and tween 60 could be appropriate nonionic surfactant for Dox entrapment. One possible explanation for this EE% is the good interaction of the drug and these surfactants.

3.7 *In vitro release experiment*

Passive transfer through the membrane bilayer due to a concentration gradient or breakdown of the carrier membrane is the most common drug release mechanism from vesicular-based nanosystems [43]. To build up an optimum drug delivery system, for example, for antineoplastic treatments, many times it is critical to accomplish sustained cargo release and extended drug retention. The release profiles of the DOX-loaded produced niosomes were analyzed by dialysis experiments and are shown in Figure 7. The drug release profile was monitored for 24 h in PBS buffer at pH 7.4 and 5.4 and 37 °C since these are the typical conditions mimicking biological plasma and in the tumor environment, respectively. Results showed that the free drug was released almost completely after 4 hours. On the other hand, Dox-loaded niosomes showed a sustainable release, so that Dox was released faster at pH 5.4 compared to pH 7.4. This phenomenon is attributed to the existence of CHEMS constituents in niosome bilayers that provide a pH-dependent release.

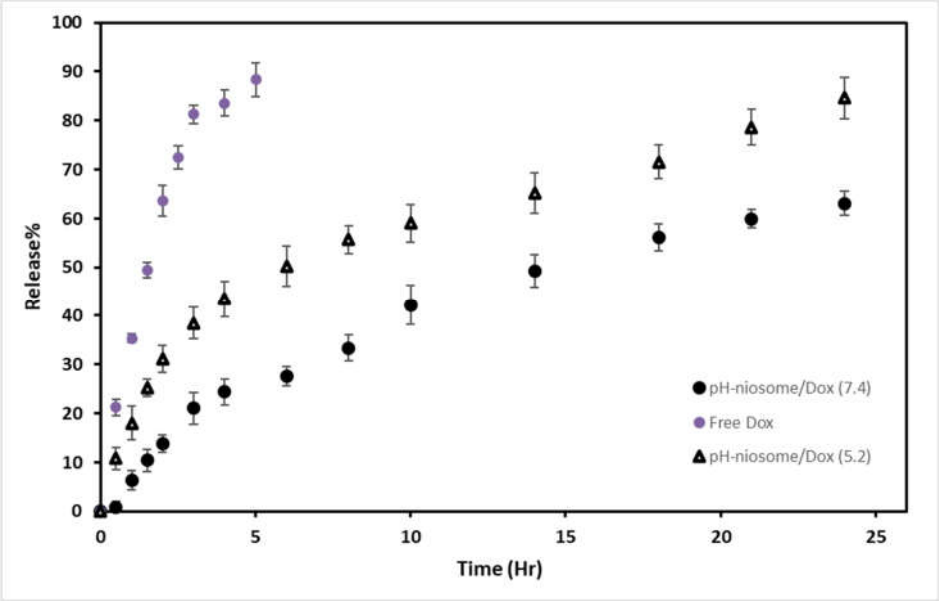

Figure 7. Cumulative release DOX at 37 ºC: (○) Free DOX, (△) pH-responsive niosomes at pH 5.4, and (●) pH-responsive niosomes at pH 7.4

3.8 *Anti-cancer activity of free and niosomal DOX*

The cytotoxic activity of DOX-loaded niosomes was evaluated by means of the MTT assay in MCF/breast cancer cells. MTT data revealed that treatment with niosomal DOX exhibited a considerable time- and concentration-dependent cell toxicity, suppressing the proliferation of the cancerous MCF7 cells ($P<0.05$ compared with control cells (see Figure 8). The percentage of viable MCF7 cells following 48 h exposure to 0.075, 0.15, 0.3, 0.6, and 1.2 µg/mL of niosomal DOX was 94.2, 72.2, 66.6, 58.6, and 49.0%, respectively, much higher than those observed for free-administered DOX at similar concentrations. IC50 values of MCF7 cells treated with free DOX were 1.15, 0.80, and 0.46 µg/mL after 24, 48, and 72 h of exposure, respectively, compared to 0.23, 0.14, and 0.08 µg/mL when cells were exposed to niosomal DOX. In addition, the exposure of MCF7 cells to an increasing concentration of free DOX for 48 h slightly diminished the number of viable cells without inducing notable morphological alterations. At the same time, significant morphological changes in MCF7 cells treated with niosomal DOX are noted: When treated with 0.3-0.6 µg/mL of niosomal DOX, cell density decreased, cells shrunk, and apoptotic

bodies are formed. At the highest concentration of niosomal DOX (1.2 µg/mL), detachment of cells from the culture plate was clearly observed, evidence of complete cell death (Figure 9).

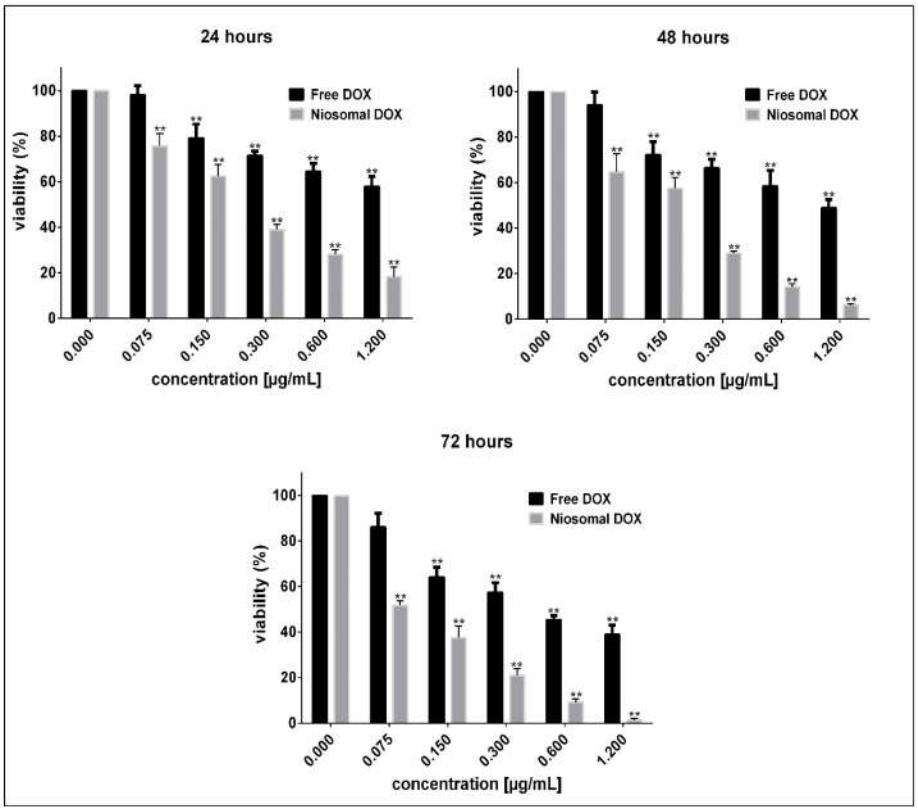

Figure 8. Cytotoxic effects of free and niosomal encapsulated DOX on breast cancer MCF7 cells. **P<0.05 compared with control cells

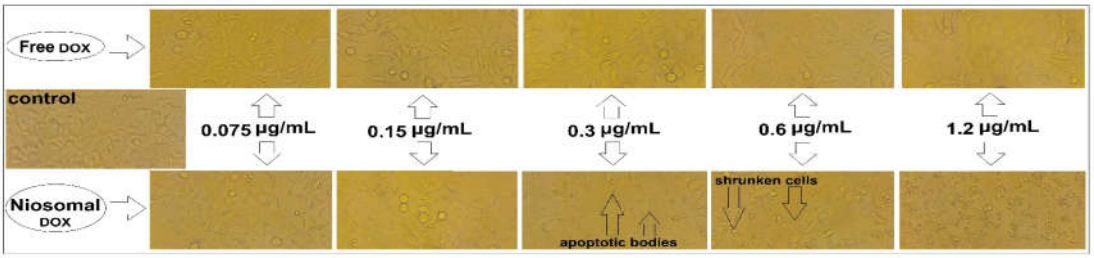

Figure 9. Optical microscopic images of MCF7 cells exposed to 0.015-1.2 µg/mL of free and niosomal encapsulated DOX

Furthermore, our cytotoxic examinations showed that niosomal DOX exerted a higher cytotoxicity effect than free-administered DOX on breast cancer cells. Besides, evident morphological changes were observed in niosomal DOX-treated MCF7 cells after 48 h. It has been previously proposed that the encapsulation of DOX in niosomes coated with different polymers enhances its anti-cancer efficacy and can be considered a novel drug delivery system for sustained drug release in treating various cancers. Bahrami-Banan prepared nano-niosomes containing DOX, examined their cytotoxic activity against KG-1 acute myeloblastic leukemia cells, and found that niosomes loaded with DOX exhibited higher cytotoxic effects than its non-encapsulated from [44]. Kulkarni et al. also suggested a profound therapeutic application of niosomes for treating breast cancer cells by co-loading DOX and

Tamoxifen. Furthermore, newly synthesized cationic PEGylated niosomes co-loaded with DOX, other anti-cancer agents, and short interfering RNAs have also yielded promising results for cancer treatment [45, 46].

4. Conclusion

We showed that niosomes are promising nanocarriers that can be employed to encapsulate Dox currently used in clinics. This can improve their therapeutic outcomes while avoiding severe adverse toxic effects. Alpha-hydroxy ketone and daunosamine moieties of DOX are responsible for its arrangement toward the niosome bilayer within the nanovehicle. At the same time, the naphthacene part governs the dimerization or higher-order oligomerization of the DOX molecule in bulk or at the interface of bilayer and solvent, stabilizing the formulation. Our newly synthesized niosomes loaded with DOX exhibited better cytotoxic effects against breast cancer cells compared with free administered DOX. These results provided evidence for using pH-responsive niosomes as promising drug delivery platforms in cancer therapy.

Conflicts of Interest

The authors declare not having competing interests.

Acknowledgments

This study received a grant from Zahedan University of Medical Sciences (Project No. 10267). P.T also thanks Agencia Estatal de Investigación (AEI) by project PID2019-109517RB-I00. ERDF funds are also acknowledged.

Availability of Data and Material

The data in this manuscript are available from the corresponding author upon reasonable request.

Ethics Approval

The *in-vitro* part of the study protocol was approved by Zahedan University of Medical Sciences (Ethical code: IR.ZAUMS.REC.1399.517).

Informed Consent

Not applicable.

References

1. Tian M, Schiemann WP. TGF-β stimulation of EMT programs elicits non-genomic ER-α activity and anti-estrogen resistance in breast cancer cells. *J. Cancer Metastasis Treat.*, 2017, 3:150.

2. Dong X, Yang A, Bai Y, Kong D, Lv F. Dual fluorescence imaging-guided programmed delivery of doxorubicin and CpG nanoparticles to modulate tumor microenvironment for effective chemo-immunotherapy. *Biomaterials*, 2020, 230:119659.

3. van der Zanden SY, Qiao X, Neefjes J. New insights into the activities and toxicities of the old anticancer drug doxorubicin. *FEBS J.*, 2021, 288(21):6095-6111.

4. Jain V, Kumar H, Anod HV, Chand P, Gupta NV, Dey S, Kesharwani SS. A review of nanotechnology-based approaches for breast cancer and triple-negative breast cancer. *J. Controlled Release*, 2020, 326:628-647.

5. Graham K, Unger E. Overcoming tumor hypoxia as a barrier to radiotherapy, chemotherapy and immunotherapy in cancer treatment. *Int. J. Nanomed.*, 2018, 13:6049.

6. Sivasankarapillai VS, Somakumar AK, Joseph J, Nikazar S, Rahdar A, Kyzas GZ. Cancer theranostic applications of MXene nanomaterials: Recent updates. *Nano-Struct. Nano-Objects*, 2020, 22:100457.

7. Mashayekhi S, Rasoulpoor S, Shabani S, Esmaeilizadeh N, Serati-Nouri H, Sheervalilou R, Pilehvar-Soltanahmadi Y. Curcumin-loaded mesoporous silica nanoparticles/nanofiber composites for supporting long-term proliferation and stemness preservation of adipose-derived stem cells. *Int. J. Pharm.*, 2020, 587:119656.

8. Shakeri-Zadeh A, Zareyi H, Sheervalilou R, Laurent S, Ghaznavi H, Samadian H. Gold nanoparticle-mediated bubbles in cancer nanotechnology. *J. Controlled Release*, 2021, 330:49-60.

9. Peer D, Karp JM, Hong S, Farokhzad OC, Margalit R, Langer R. Nanocarriers as an emerging platform for cancer therapy. *in*: Nano-Enabled Medical Applications. Balogh LP (Ed). 1st ed., Dubai: Jenny Stanford Publishing, 2020, pp 61-91.

10. Veiga N, Diesendruck Y, Peer D. Targeted lipid nanoparticles for RNA therapeutics and immunomodulation in leukocytes. *Adv. Drug Delivery Rev.*, 2020, 159:364-376.

11. Garcia-Fuentes M, Torres D, Alonso MJ. New surface-modified lipid nanoparticles as delivery vehicles for salmon calcitonin. *Int. J. Pharm.*, 2005, 296(1-2):122-132.

12. Hou D, Xie C, Huang K, Zhu C. The production and characteristics of solid lipid nanoparticles (SLNs). *Biomaterials*, 2003, 24(10):1781-1785.

13. Chen R, Wang S, Zhang J, Chen M, Wang Y. Aloe-emodin loaded solid lipid nanoparticles: formulation design and in vitro anti-cancer study. *Drug Delivery*, 2015, 22(5):666-674.

14. Sriraman SK, Salzano G, Sarisozen C, Torchilin V. Anti-cancer activity of doxorubicin-loaded liposomes co-modified with transferrin and folic acid. *Eur. J. Pharm. Biopharm.*, 2016, 105:40-49.

15. Kim K, Oh KS, Park DY, Lee JY, Lee BS, San Kim I, Kim K, Kwon IC, Sang YK, Yuk SH. Doxorubicin/gold-loaded core/shell nanoparticles for combination therapy to treat cancer through the enhanced tumor targeting. *J. Controlled Release*, 2016, 228:141-149.

16. Duong VA, Nguyen TTL, Maeng HJ. Preparation of solid lipid nanoparticles and nanostructured lipid carriers for drug delivery and the effects of preparation parameters of solvent injection method. *Molecules*, 2020, 25(20):4781.

17. Rahdar A, Sargazi S, Barani M, Shahraki S, Sabir F, Aboudzadeh MA. Lignin-stabilized doxorubicin microemulsions: Synthesis, physical characterization, and in vitro assessments. *Polymers*, 2021, 13(4):641.

18. Rahdar A, Hajinezhad MR, Barani M, Sargazi S, Zaboli M, Ghazy E, Baino F, Cucchiarini M, Bilal M, Pandey S. Pluronic F127/Doxorubicin microemulsions: Preparation, characterization, and toxicity evaluations. *J. Mol. Liq.*, 2022, 345:117028.

19. Bhardwaj P, Tripathi P, Gupta R, Pandey S. Niosomes: A review on niosomal research in the last decade. *J. Drug Delivery Sci. Technol.*, 2020, 56:101581.

20. Ruman U, Fakurazi S, Masarudin MJ, Hussein MZ. Nanocarrier-based therapeutics and theranostics drug delivery systems for next generation of liver cancer nanodrug modalities. *Int. J. Nanomed.*, 2020, 15:1437.

21. Wibowo FR, Saputra OA, Lestari WW, Koketsu M, Mukti RR, Martien R. pH-triggered drug release controlled by poly (styrene sulfonate) growth hollow mesoporous silica nanoparticles. *ACS Omega*, 2020, 5(8):4261-4269.

22. Maity D, Sudame A, Kandasamy G. Superparamagnetic Iron Oxide Nanoparticle-Based Drug Delivery in Cancer Therapeutics. *in*: Nanobiotechnology in Diagnosis, Drug Delivery and Treatment. Rai M, Razzaghi-Abyaneh M, Ingle AP. (Eds). 1st ed., Hoboken: Wiley-Blackwell, 2020, pp 129-151.

23. Manspeaker MP, Thomas SN. Lymphatic immunomodulation using engineered drug delivery systems for cancer immunotherapy. *Adv. Drug Delivery Rev.*, 2020, 160:19-35.

24. Chen F, Smith PE. Simulated surface tensions of common water models. *J. Chem. Phys.*, 2007, 126(22):221101.

25. van Gunsteren WF, Berendsen HJ. Groningen molecular simulation (GROMOS) library manual. *Biomos Groningen*, 1987, 24(682704):13.

26. Schmid N, Eichenberger AP, Choutko A, Riniker S, Winger M, Mark AE, van Gunsteren WF. Definition and testing of the GROMOS force-field versions 54A7 and 54B7. *Eur. Biophys. J.*, 2011, 40(7):843-856.

27. Malde AK, Zuo L, Breeze M, Stroet M, Poger D, Nair PC, Oostenbrink C, Mark AE. An automated force field topology builder (ATB) and repository: version 1.0. *J. Chem. Theory Comput.*, 2011, 7(12):4026-4037.

28. Nasseri B. Effect of cholesterol and temperature on the elastic properties of niosomal membranes. *Int. J. Pharm.*, 2005, 300(1-2):95-101.

29. Baranyai A, Evans DJ. New algorithm for constrained molecular-dynamics simulation of liquid benzene and naphthalene. *Mol. Phys.*, 1990, 70(1):53-63.

30. Berendsen HJ, van der Spoel D, van Drunen R. GROMACS: a message-passing parallel molecular dynamics implementation. *Comput. Phys. Commun.*, 1995, 91(1-3):43-56.

31. Barani M, Nematollahi MH, Zaboli M, Mirzaei M, Torkzadeh-Mahani M, Pardakhty A, Karam GA. In silico and in vitro study of magnetic niosomes for gene delivery: The effect of ergosterol and cholesterol. *Mater. Sci. Eng. C*, 2019, 94:234-246.

32. Heydari M, Yousefi AR, Rahdar A, Nikfarjam N, Jamshidi K, Bilal M, Taboada P. Microemulsions of tribenuron-methyl using Pluronic F127: Physico-chemical characterization and efficiency on wheat weed. *J. Mol. Liq.*, 2021, 326:115263.

33. Rahdar A, Taboada P, Aliahmad M, Hajinezhad MR, Sadeghfar F. Iron oxide nanoparticles: Synthesis, physical characterization, and intraperitoneal biochemical studies in Rattus norvegicus. *J. Mol. Struct.*, 2018, 1173:240-245.

34. Salimi A, Zadeh BSM, Godazgari S, Rahdar A. Development and Evaluation of Azelaic Acid-Loaded Microemulsion for Transfollicular Drug Delivery Through Guinea Pig Skin: A Mechanistic Study. *Adv. Pharm. Bull.*, 2020, 10(2):239.

35. Nguyen TT, Shklovskii BI. Complexation of DNA with positive spheres: phase diagram of charge inversion and reentrant condensation. *J. Chem. Phys.*, 2001, 115(15):7298-7308.

36. Bordi F, Cametti C, Diociaiuti M, Sennato S. Large equilibrium clusters in low-density aqueous suspensions of polyelectrolyte-liposome complexes: a phenomenological model. *Phys. Rev. E*, 2005, 71(5):050401.

37. Allen WJ, Lemkul JA, Bevan DR. GridMAT-MD: a grid-based membrane analysis tool for use with molecular dynamics. *J. Comput. Chem.*, 2009, 30(12):1952-1958.

38. Peltonen L, Hirvonen J, Yliruusi J. The effect of temperature on sorbitan surfactant monolayers. *J. Colloid Interface Sci.*, 2001, 239(1):134-138.

39. Menozzi M, Valentini L, Vannini E, Arcamone F. Self-Association of Doxorubicin and Related Compounds in Aqueous Solution. *J. Pharm. Sci.*, 1984, 73(6):766-770.

40. Anand R, Ottani S, Manoli F, Manet I, Monti S. A close-up on doxorubicin binding to γ-cyclodextrin: an elucidating spectroscopic, photophysical and conformational study. *RSC Adv.*, 2012, 2(6):2346-2357.

41. Hayakawa E, Furuya K, Kuroda T, Moriyama M, Kondo A. Viscosity Study on the Self-Association of Doxorubicin in Aqueous Solution. *Chem. Pharm. Bull.*, 1991, 39(5):1282-1286.

42. Ritwiset A, Krongsuk S, Johns JR. Molecular structure and dynamical properties of niosome bilayers with and without cholesterol incorporation: A molecular dynamics simulation study. *Appl. Surf. Sci.*, 2016, 380:23-31.

43. Momekova DB, Gugleva VE, Petrov PD. Nanoarchitectonics of Multifunctional Niosomes for Advanced Drug Delivery. *ACS Omega*, 2021, 6(49):33265-33273.

44. Bahrami-Banan F, Sheikhha MH, Ghasemi N, Majdizadeh M, Haghiralsadat BF. Preparation and study of nano-niosomes containing doxorubicin and evaluation of its toxicity on acute myeloblastic leukemia cell line KG-1. *J. Payavard Salamat*, 2018, 12(4):309-323.

45. Kulkarni P, Rawtani D. Application of Box-Behnken Design in the Preparation, Optimization, and In Vitro Evaluation of Self-assembly–based Tamoxifen- and Doxorubicin-loaded and Dual Drug–loaded Niosomes for Combinatorial Breast Cancer Treatment. *J. Pharm. Sci.*, 2019, 108(8):2643-2653.

46. Hemati M, Haghiralsadat F, Jafary F, Moosavizadeh S, Moradi A. Targeting cell cycle protein in gastric cancer with CDC20siRNA and anticancer drugs (doxorubicin and quercetin) co-loaded cationic PEGylated nanoniosomes. *Int. J. Nanomed.*, 2019, 14:6575.

How to cite this article: Sargazi S, Barani M, Zargari F, Arshad R, Sharma RK. Preparation of pH-Responsive Vesicular Doxorubicin: Evidence from In-Vitro and In-Silico Evaluations. *Curr. Appl. Sci.*, 2022, 2(1):31-48. https://doi.org/10.22034/cas.2022.346726.1024